A&A 662, A73 (2022)
https://doi.org/10.1051/0004-6361/202243431

Astronomy & Astrophysics

Lyα irradiation of solid-state formamide

T. Suhasaria[1,2] and V. Mennella[2]

[1] Max Planck Institute für Astronomie, Königstuhl 17, 69117 Heidelberg, Germany
e-mail: suhasaria@mpia.de
[2] INAF-Osservatorio Astronomico di Capodimonte, Salita Moiariello 16, 80131 Naples, Italy

Received 28 February 2022 / Accepted 18 March 2022

ABSTRACT

Context. Formamide (NH_2CHO) has been proposed as a potential prebiotic precursor in the scientific discourse on the origin of life. It has been observed in different environments in space, including protostellar regions and comets. The abundance and stability of NH_2CHO in the early stages of star formation can be better understood by incorporating the formation and destruction data in astrochemical models.
Aims. We carried out an experimental investigation to study the destruction of pure NH_2CHO ice at 12 K as a result of the interaction with Lyα (121.6 nm) photons.
Methods. We studied UV photo destruction of NH_2CHO using Fourier-transform infrared spectroscopy.
Results. After UV processing, the intensity of NH_2CHO IR bands decreased and new bands corresponding to HCN, CO, NH_4^+ OCN^-, HNCO, and CO_2 appeared in the spectrum. We then derived the destruction and cumulative product formation cross-sections.
Conclusions. A comparison of destruction rates derived from the cross-section in a cold and dense molecular cloud for different energetic processing agents reveals that UV photons induce NH_2CHO destruction at a level that is one order of magnitude greater than that affected by cosmic rays; however, it is three orders of magnitude lower than that of H atoms.

Key words. astrochemistry – methods: laboratory: solid state – techniques: spectroscopic – ISM: molecules – ultraviolet: ISM

1. Introduction

Formamide (NH_2CHO) is one of the simplest molecules to contain the four primary biogenic elements and an amide bond. It is considered a promising precursor molecule in the context of the origin of life on our planet (Saladino et al. 2012). Formamide chemistry in a controlled terrestrial environment allows for the formation of essential biological life components such as amino acids, nucleobases, sugars, and carboxylic acids (Saladino et al. 2012; Ferus et al. 2015; Botta et al. 2018). Moreover, it has been observed in many astrophysical environments such as galactic centres, star-forming regions, and comets (e.g., Blake et al. 1986; Turner 1991; Bisschop et al. 2007; Mendoza et al. 2014; López-Sepulcre et al. 2015; Bockelée-Morvan et al. 2000; Biver et al. 2014; Goesmann et al. 2015). In fact, the mass spectrometric analysis by COmetary Sampling And Composition (COSAC), aboard Rosetta's Philae lander on comet 67P/Churyumov–Gerasimenko, revealed that NH_2CHO (1.8% with respect to water) is the second-most abundant molecule after H_2O (Goesmann et al. 2015; Altwegg et al. 2017). Solid-state NH_2CHO has also been identified tentatively in the interstellar medium by the Infrared Space Observatory towards NGC 7538 IRS9 and W33A (Raunier et al. 2004a; Gibb et al. 2004).

Based on experimental and theoretical studies, it has been proposed that NH_2CHO was formed in space by a series of ion-molecule and neutral-neutral reaction channels in the gas phase, whereas solid NH_2CHO could be formed via a processing of interstellar ices on dust grain surface by electrons, ions, ultraviolet (UV) photons, heat, and H atoms (López-Sepulcre et al. 2019, and references therein). Once formed, NH_2CHO can undergo further processing both in the gas or solid phase to form simple and complex organic molecules. As a result, the abundance of NH_2CHO in a certain space environment will depend both on the formation and destruction channels. Therefore, understanding the destruction channels of NH_2CHO under energetic and non-energetic processing has been the subject of numerous studies.

Quantum mechanical calculations on the thermal decomposition of NH_2CHO revealed three main reaction channels (Nguyen et al. 2011). In decreasing order of kinetically favoured pathways, these are: dehydration (H_2O loss to hydrogen cyanide (HCN)), decarbonylation (carbon monoxide (CO) loss to ammonia (NH_3)), and dehydrogenation (hydrogen (H_2) loss to isocyanic acid (HNCO)). A high-energy laser spark induces the decomposition of NH_2CHO gas to HCN, CO, NH_3, carbon dioxide (CO_2), nitrous oxide (N_2O), hydroxylamine ($HONH_2$), and methanol (CH_3OH), which was identified by infrared (IR) spectroscopy (Ferus et al. 2011). The NH_2CHO decomposition in matrices also leads to similar products as observed in the gas-phase reactions (Lundell et al. 1998; Maier & Endres 2000; Duvernay et al. 2005). A limited number of studies have been dedicated to investigate the destruction of NH_2CHO in the condensed phase. Ion irradiation experiments with 200 keV H^+ were performed on NH_2CHO films deposited on inert silicon and olivine substrate (Brucato et al. 2006a,b). An IR analysis showed the formation of CO, CO_2, NH_3, N_2O, HCN, cyanide ion (CN^-), ammonium ion (NH_4^+), isocyanate ion (OCN^-), and isocyanic acid (HNCO) on silicon whereas all the other products except CN^- and NH_3 were formed on the olivine surface. In a different set of experiments, pure NH_2CHO films show no significant degradation upon processing by UV-enhanced xenon lamp, whereas oxide minerals titanium dioxide (TiO_2) and spinel ($MgAl_2O_4$) used as substrates induce a gradual but

minimal degradation (Corazzi et al. 2020). On the other hand, Lyman (Ly)α photons and 1 keV electron bombardment of amorphous or crystalline NH_2CHO film deposited on silica (SiO_2) nanopowder at 70 K revealed only OCN^- and CO (Dawley et al. 2014a).

More recently, two independent investigations were made to study the reaction of H atoms on NH_2CHO ice (Haupa et al. 2019; Suhasaria & Mennella 2020). Haupa et al. (2019) showed that HNCO was formed through H-abstraction reactions via a H_2NCO radical intermediate when NH_2CHO was subject to H atoms in the para-hydrogen quantum-solid matrix host. Furthermore, Suhasaria & Mennella (2020) studied the effect of H atom exposure on NH_2CHO at 12 K to estimate the effective destruction cross-section. This quantity was used to evaluate the destruction rate of NH_2CHO by H atoms in space and was then compared with the destructive effects of cosmic rays and UV photons. However, the absence of destruction cross-section for NH_2CHO under Lyα (10.2 eV) photons only allowed the estimation of an upper limit for the destruction rate under interstellar medium conditions. The present study reports the results of the interaction of Lyα with pure NH_2CHO ice film at 12 K. The NH_2CHO destruction and new products formed after UV irradiation have been studied by Fourier-transform infrared (FTIR) spectroscopy. The destruction cross-section for NH_2CHO and the cumulative formation cross-section for the formed new species have been obtained. The determination of the destruction cross-section has then allowed us to compare the destructive effects of H atoms, cosmic rays, and UV photons on pure solid NH_2CHO in dense interstellar cloud conditions.

2. Experimental methods

Experiments were performed in a high vacuum chamber, which is described in detail in previous works (Mennella et al. 2006; Suhasaria & Mennella 2020). The salient features of the set-up relevant to this work are briefly described here. The main chamber, with a base pressure better than 10^{-8} mbar, is equipped with a closed-cycle helium cryostat and a dosing unit. A caesium iodide (CsI) substrate was mounted on the cold finger of the cryostat such that the substrate can be cooled down to 12 K. Then, NH_2CHO (EMSURE grade; Merck) was purified by several freeze-pump-thaw and deposited on the substrate from the dosing unit with a pressure better than 10^{-6} mbar. The ice film deposition is expected to be non-homogeneous.

To study the effects induced by UV photons, the NH_2CHO ice film was irradiated using a microwave excited hydrogen flow discharge lamp attached to the main chamber with a magnesium fluoride (MgF_2) window. The Lyα (10.2 eV) emission accounts for 97% of the total UV emission of the source (Mennella et al. 2006). The UV beam forms an angle of 22.5° with the normal to the substrate. During sample irradiation, the UV flux (fluence) was monitored by measuring the current (charge) generated by photoelectric effect on a platinum wire inserted between the source and the substrate. Details on the calibration of the wire sensor and on the measure of the flux at the substrate position are given in Mennella et al. (2006).

The NH_2CHO ice film was studied in situ before and during irradiation in transmittance mode in the mid-infrared range at a resolution of 2 cm^{-1} using a FTIR spectrometer (Bruker Vertex 80V) with a Mercury Cadmium Telluride (MCT) detector. For each single measurement, 1024 scans were co-added. The background was acquired for any spectral measurement of NH_2CHO before and after each irradiation step.

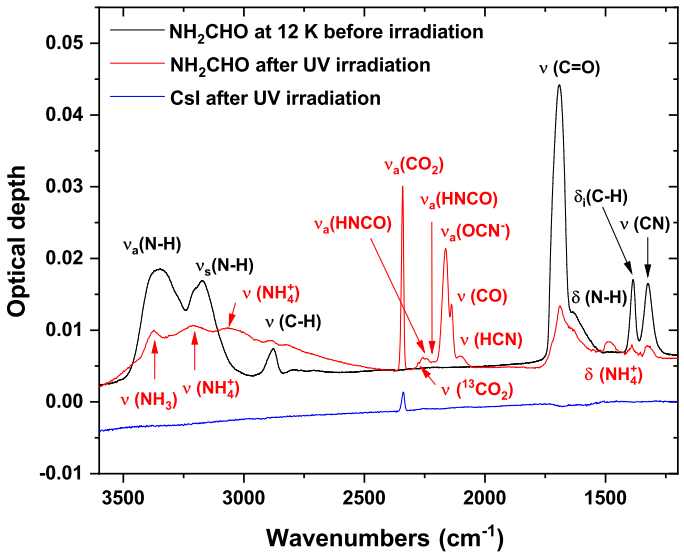

Fig. 1. Mid-IR spectrum of a 29.5 ML thick NH_2CHO film at 12 K as deposited (black line) and after UV irradiation of 6.5×10^{18} photons cm^{-2} (red line). Symbols ν and δ stand for stretching and bending modes, respectively. The subindex a, s, and i denotes antisymmetric, symmetric, and in-plane mode, respectively. The spectrum of a CsI substrate after UV irradiation of 6.5×10^{18} photons cm^{-2} (blue line) is also shown for comparison. The red and blue curves are offset in ordinate by 0.0055 and −0.005, respectively, for the sake of clarity.

3. Results and discussion

3.1. Ice growth

The IR spectrum of pure solid NH_2CHO at 12 K is displayed in Fig. 1 and the corresponding fundamental vibration modes reported in Table 1 are in good agreement with the previous results (Brucato et al. 2006a; Suhasaria & Mennella 2020). The NH_2CHO ice film thickness was derived separately from the column density of combined symmetric and antisymmetric N–H, C–H, and C=O stretching IR modes using the band strengths values listed in Table 1. The average value, expressed in units of monolayer (1 ML = 10^{15} molecules cm^{-2}), is 29.5 ML which is equivalent to 0.03 μm. For the thickness determination, we took into account the cosine of the angle between the IR beam and the normal to the surface plane and the NH_2CHO ice density 0.937 g cm^{-3} derived by Brucato et al. (2006a). The NH_2CHO ice thickness was found to be below the UV penetration depth since the mean free path of UV photons, d_{UV}, through the NH_2CHO films has been estimated to be 0.04 μm. The mean free path of UV photons was derived using the relation, $d_{UV} = 1/\beta = 1/\sigma n$, where β is the absorption coefficient, σ is the UV photoabsorption cross-section of NH_2CHO, and n is the number of NH_2CHO molecules per unit volume. In the absence of direct measurements of the UV absorption cross-section for NH_2CHO ice, the gas phase value of ca. 2×10^{-17} cm^2 (Gingell et al. 1997) acquired at 10.2 eV photons is taken into the calculation.

3.2. UV irradiation of NH_2CHO

Figure 1 also presents the IR spectrum of NH_2CHO ice after exposure to UV photon fluence of 6.5×10^{18} photons cm^{-2}. The intensity decrease of the NH_2CHO IR bands indicates that the NH_2CHO ice was depleted. At the same time, several new bands appear in the spectrum. The most intense band at 2341 cm^{-1} band is due to the asymmetric stretch mode of CO_2. The second

Table 1. IR absorption band positions of pure NH_2CHO ice and the new species formed after the UV irradiation of NH_2CHO.

Molecule	Band position (cm^{-1})	Vibration mode	Band strength (cm molecule^{-1})
NH_2CHO	3355	ν_a (N–H)	1.4×10^{-16} (a)
	3170	ν_s (N–H)	
	2878	ν (C–H)	4.7×10^{-18}
	1690	ν (C=O)	6.5×10^{-17}
	1631	δ (N–H)	
	1386	δ_i (C–H)	
	1324	ν (CN)	
NH_3	3375	ν (N–H)	
NH_4^+	3210	ν (N–H)	
	3065	ν (N–H)	
	1483	δ (N–H)	
CO_2	2341	ν_a (C–O)	7.6×10^{-17} (b)
$^{13}CO_2$	2277	ν_a (C–O)	
HNCO	2259	ν_a (N=C=O)	7.2×10^{-17} (c)
	2240	ν_a (N=C=O)	
OCN^-	2163	ν_a (N=C=O)	1.3×10^{-16} (c)
CO	2138	ν (C≡O)	1.1×10^{-17} (d)
HCN	2100	ν (C≡N)	1.1×10^{-17} (e)

Notes. Only the band strengths of those modes are reported when the respective column densities were evaluated. (a)The band strength corresponds to ($\nu_a + \nu_s$). All the band strength values are taken from Brucato et al. (2006a). (b)Yamada & Person (1964). (c)Van Broekhuizen et al. (2004). (d)Jiang et al. (1975). (e)Gerakines et al. (2022).

most intense band at 2163 cm^{-1} shows a good agreement with the expected frequency of the N=C=O asymmetric stretching mode of OCN^- (Gerakines et al. 2004). The counter ion NH_4^+ was clearly identified from the very broad N–H IR bending mode feature around 1483 cm^{-1} (Raunier et al. 2004a). Further evidence for the presence of NH_4^+ ion comes from the broad features at 3210 and 3065 cm^{-1} overlapping with formamide N–H stretching modes. These peaks are in close agreement with the NH_4^+ peaks at 3206 and 3074 cm^{-1} assigned previously by Brucato et al. (2006a).

At 2138 cm^{-1}, there is the symmetric stretch feature of CO which appears as a shoulder to the OCN^- peak. The band observed at 2259 cm^{-1} and a shoulder peak at the lower wavenumber side, centred around 2240 cm^{-1}, were assigned to the N=C=O asymmetric stretching mode of HNCO (Raunier et al. 2004b). The shoulder peak at 2240 cm^{-1} could also be associated with the N=N stretching mode of N_2O (Brucato et al. 2006a). Furthermore, a shoulder peak at the higher wavenumber side of the 2259 cm^{-1} band, centred around 2277 cm^{-1}, is attributed to $^{13}CO_2$ (Modica & Palumbo 2010). Within the errors, the natural abundance ratio of ^{13}C:^{12}C = 0.011 is in agreement with the band area ratio of $^{13}CO_2$:$^{12}CO_2$ = 0.015. A peak around 2100 cm^{-1} has been assigned previously to the C≡N stretching mode of HCN (Brucato et al. 2006a). The 2100 cm^{-1} band is the second strongest IR band of pure solid HCN ice after 3115 cm^{-1} (Couturier-Tamburelli et al. 2018), which has not been identified in the present experiment but could be obscured by the broad stretching band of N-H in NH_2CHO. Also, NH_3 has been tentatively identified after UV irradiation from the band present at 3375 cm^{-1} due to N–H stretching based on the assignment by Brucato et al. (2006a). The band positions of the newly formed species are reported in Table 1. A control

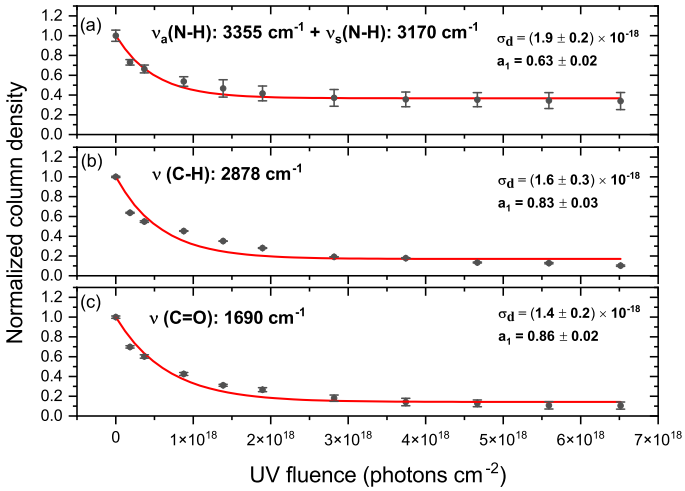

Fig. 2. Evolution with UV photon fluence of the N–H (*a*), C–H (*b*) and C=O (*c*) normalised column density (filled circles). The normalisation factor is the corresponding initial column densities. The error arising due to baseline subtraction was taken into the error estimation. When the error bar is not visible, the error is within the size of the filled circle. The best fit to the data (red solid lines) is also shown. The estimated destruction cross-section (σ_d) and the asymptotic destruction (a_1) for NH_2CHO are also reported.

experiment was also performed where a bare substrate was subjected to the same UV photon fluences as NH_2CHO ice. In this case, a stretching mode for CO_2 was observed. At the maximum fluence, its intensity accounts for 12.5% of the CO_2 band observed in the formamide irradiation (see Fig. 1).

Figure 2 shows the evolution of normalised column densities, $\tau(t)$, of N–H, C–H, and C=O stretching modes of NH_2CHO as a function of UV photon fluence, F_{UV}. The experimental data was fitted following first order kinetic relation:

$$\tau(t) = [1 - a_1(1 - e^{-\sigma_d F_{UV}})]. \quad (1)$$

The equation refers to the destruction with the boundary condition that considers a residual reactant for $F_{UV} = \infty$. Fits to the experimental data in Fig. 2 allowed us to estimate the cross-sections and asymptotic values for the NH_2CHO destruction (σ_d, a_1). The destruction cross-section estimated from the three stretch modes are equal within the errors, suggesting that there is no difference in the chemical bond cleavage of corresponding functional groups upon irradiation by UV photons. This result differs from what we have found during H atoms exposure to NH_2CHO, where the C–H bonds are cleaved by H atom abstraction before the N–H bonds of the NH_2 group (Suhasaria & Mennella 2020). The estimated destruction cross-section was in agreement with the preliminary values obtained for formamide destruction by Lyα photons in an entirely different set-up (Escobar & Ciaravella, priv. comm.). The average of the three estimated asymptotic fit parameters $a_{1,N-H}$, $a_{1,CH}$, and $a_{1,CO}$ is 0.77 that corresponds to the destruction of 22.7 ML of the initial NH_2CHO ice. In the Lyα irradiation experiments of NH_2CHO deposited on SiO_2 nanoparticles, after a UV photon fluence of 7×10^{19} photons cm^{-2}, ca. 29% of the initial NH_2CHO ice was destroyed (Dawley et al. 2014b). On the other hand, ion irradiation of NH_2CHO leads to the destruction of 64 and 78% of the initial NH_2CHO molecules at fluences of 6.8×10^{14} and 1.4×10^{15} ions cm^{-2}, respectively (Brucato et al. 2006a).

The evolution of the column density of newly formed photo products normalised to the initial column density of NH_2CHO

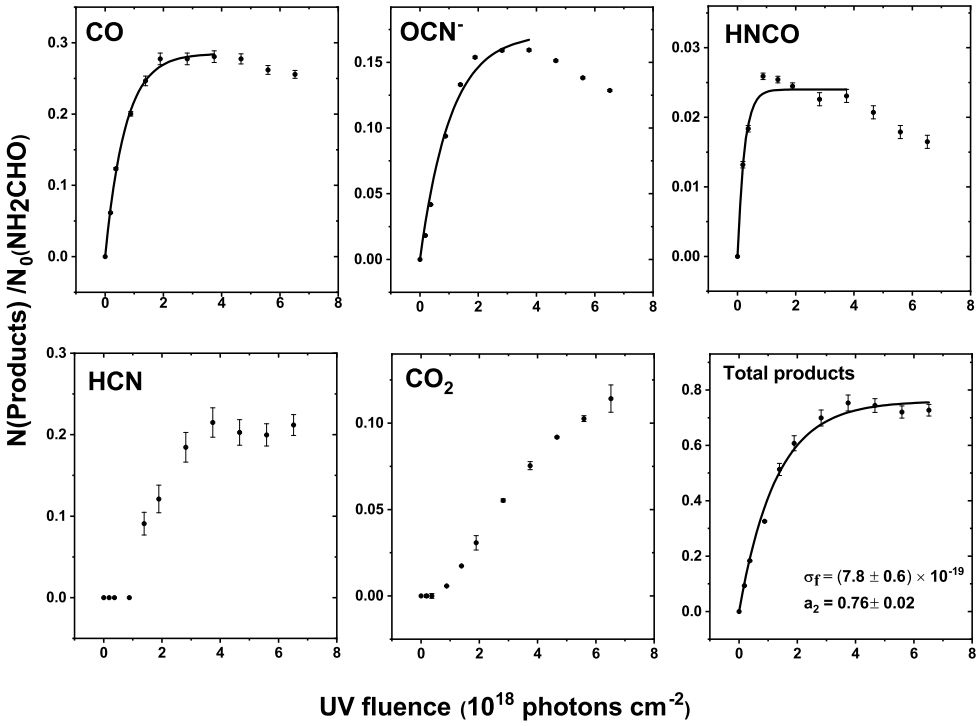

Fig. 3. Evolution of normalised column density of different photo products with increasing UV photon fluence. The normalisation factor is the column density of NH_2CHO before UV irradiation. The IR absorption area is obtained by Gaussian fitting, with one standard deviation used as an error bar. When the error bar is not visible, the error is within the size of the symbol. The best fit to the cumulative abundance growth of the total photo product (solid black line) is also shown. The estimated formation cross-section (σ_f) and asymptotic formation (a_2) are also reported. Similarly, the best fit to the growth curves (till $F_{UV} = 3.7 \times 10^{18}$ photons cm^{-2}) of CO, OCN^-, and HNCO is also shown.

ice film as a function of UV fluence is shown in Fig. 3. The band strength values used in the calculation of the individual column densities of the photo products are also listed in Table 1. Some photo products display similar behaviours while others vary drastically with the increasing F_{UV}. CO, OCN^-, and HNCO are formed immediately and rapidly at the beginning of the UV photolysis, followed by a process of slowing down and plateau within the error at UV fluence of about 4×10^{18} photons cm^{-2}. As the F_{UV} increases further, there is a decrease in the formation of all the three species. The formation of CO, OCN^-, and HNCO after UV irradiation of deposited NH_2CHO, followed by a decrease in their intensity at the highest fluence is also clearly visible in the difference IR spectra in Fig. 4. On the other hand, HCN shows a delayed formation with respect to CO, OCN^- and HNCO, while HCN appears only after UV photon fluence of 1.4×10^{18} photons cm^{-2}, but then the abundance increases rapidly and the normalised column densities are close to that of CO and OCN^-. Within the error, there is no apparent sign of a decrease in HCN formation at high fluences, as evident in Figs. 3 and 4. In the case of CO_2, there is an initial phase of slow formation with increasing F_{UV} and it is only after a UV fluence of 1.9×10^{18} photons cm^{-2} that CO_2 starts to increase rapidly. We can clearly see in Fig. 4 that CO_2 intensity at the highest UV fluence increases with respect to that at 1.9×10^{18} photons cm^{-2}.

It is difficult to fit the abundance evolution of individual products over the entire UV fluence range by a single kinetic equation, due to the simultaneous formation and depletion behaviour. Therefore, following Chuang et al. (2021) a single first order kinetic relation was fitted to the cumulative abundance of all the photo products ($\chi(t)$):

$$\chi(t) = a_2(1 - e^{-\sigma_f F_{UV}}), \quad (2)$$

where σ_f is the formation cross-section and a_2 is the asymptotic formation. Fits to the experimental data allowed us to estimate the effective formation cross-section, $\sigma_f = 7.8 \pm 0.6 \times 10^{-19}$ cm^2, and the asymptotic value, $a_2 = 0.76 \pm 0.02$, for the product formation. The asymptotic value of total product formation with respect to the initial formamide column density exactly matches the average formamide destruction of 0.77. Of course, there could be other minor species produced in the irradiation experiment that have not clearly been identified by IR spectroscopy.

In the Lyα processing reactions of pure NH_2CHO ice deposited on SiO_2 nanopowder, cross-sections $\sigma_{f,CO} = 3.9 \times 10^{-20}$ and $\sigma_{f,OCN^-} = 3.6 \times 10^{-20}$ cm^2 were estimated for the formation of CO and OCN^-, respectively (Dawley et al. 2014a). Furthermore, in our previous study (Suhasaria & Mennella 2020) we estimated the effective formation cross-section of HNCO due to H atoms exposure of formamide to be $\sigma_{f,HNCO} = 4.4 \times 10^{-17}$ cm^2. Therefore, for the sake of comparison, we tried to fit only the individual growth curves of CO, OCN^-, and HNCO up to the UV fluence of 3.7×10^{18} photons cm^{-2} using the same exponential equation as used for the cumulative growth. We derived the formation cross-sections of $\sigma_{f,CO} = 1.5 \pm 0.1 \times 10^{-18}$, $\sigma_{f,OCN^-} = 1 \pm 0.1 \times 10^{-18}$, and $\sigma_{f,HNCO} = 4.2 \pm 0.5 \times 10^{-18}$ cm^2 for CO, OCN^-, and HNCO, respectively. The CO and OCN^- formation cross-sections are two orders of magnitude higher than those estimated by Dawley et al. (2014a). The above two experiments differ in surface temperature and the surface type that impacts the formation cross-section. Out of the two, the primary impact would be of the surface temperature since there is an increase in the radical recombination efficiency with temperature as radicals diffuse faster within the ice. This would result in lower formation of CO and OCN^- from NH_2CHO at a higher surface temperature. On the other hand, the impact of SiO_2 nanoparticle surface could be less relevant since 600 ML thick ice was deposited on top of the surface for UV irradiation experiment. The HNCO formation cross-section that we derived in this experiment is an order of magnitude lower than that obtained previously by the exposure of H atoms on formamide (Suhasaria & Mennella 2020). The lower value of the HNCO formation cross-section can be taken as an indirect

measure of the lesser stability of formamide under H atoms exposure compared to UV photons.

In Fig. 3, we see that the growth curves of all the photo products, apart from CO_2, resemble a first-order kinetic behaviour, except for the very high fluences, which indicates that they must be formed directly from NH_2CHO. Furthermore, CO_2 could have been formed by the effect of UV photons on CO and H_2O molecules formed in the reaction network (Watanabe & Kouchi 2002). This may explain why CO_2 formation rate is low at the initial fluence and increases only when more CO is produced in the ice mixture. At the highest UV fluence, there is not only a small decrease in the intensity of NH_2CHO but also of all the newly formed photo products except CO_2 and HCN. This suggests that in addition to NH_2CHO, there is a processing of those species produced in the ice mixture at the highest fluence, hinting that there is a complex reaction network at play. It is beyond the scope of the present work to decipher such a complex reaction network or to discuss every possible route to molecule formation.

Despite the complexity in the reaction network, the following plausible reaction pathways have been proposed based on the kinetic theory calculations by Nguyen et al. (2011). For the formation of CO, the C–N bond in NH_2CHO should be dissociated and could have proceeded either in single step or energetically favourable two step process involving aminohydroxy carbene intermediate (NH_2–C̈–OH). We tentatively identified NH_3 in the formamide spectrum after UV irradiation, as discussed above:

$$NH_2CHO \xrightarrow{h\nu} NH_2\ddot{C}OH \rightarrow CO + NH_3. \quad (3)$$

Then, HNCO should be formed by H_2 loss and proceeds either through energetically favourable single step 1,2–H_2 elimination or a two-step process:

$$NH_2CHO \xrightarrow{h\nu} HNCO + H_2. \quad (4)$$

We find that HCN can be formed as a result of the H_2O loss from NH_2CHO. The delayed formation of HCN seems to be in agreement with a multi-step formation process via a formimidic acid (HN=CH–OH) conformer as proposed by Nguyen et al. (2011):

$$NH_2CHO \xrightarrow{h\nu} HNCHOH \rightarrow HCN + H_2O. \quad (5)$$

Three specific routes have been suggested for the formation of OCN^- in the condensed phase from the UV irradiation of NH_2CHO ice (Dawley et al. 2014a). The first is the direct photodissociation followed by ionisation reaction, the second is direct ionisation followed by ion-electron recombination and electron capture, and the third is a direct dissociative electron attachment (preceded by a direct excitation in formamide, indicated by an asterix):

$$NH_2CHO \xrightarrow{h\nu} OCN^- + H_2 + H^+, \quad (6)$$

$$NH_2CHO \xrightarrow{h\nu} NH_2CHO^{\cdot+} \rightarrow OCN^- + H_2, \quad (7)$$

$$e^- + NH_2CHO \rightarrow (HNCHOH)^{*+} \rightarrow OCN^- + H_2 + H. \quad (8)$$

Since we cannot rule out any possibilities, any of the three, or even all three, reactions could potentially yield OCN^- in our study.

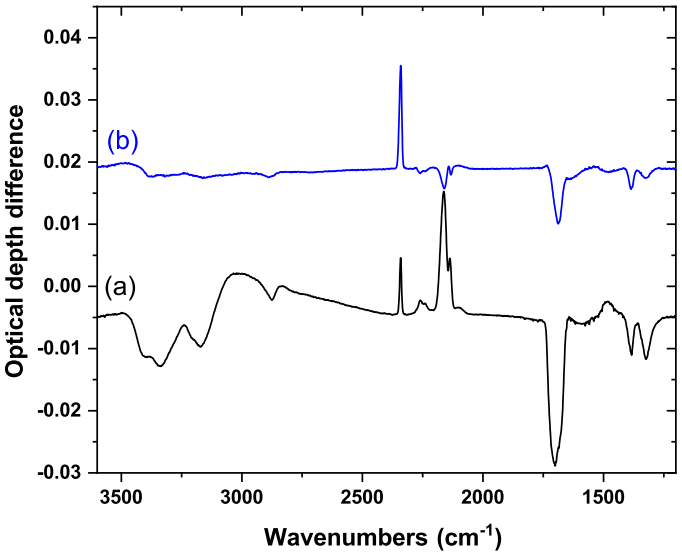

Fig. 4. Difference in the IR spectrum of NH_2CHO after UV irradiation of: (*a*) 1.9×10^{18} photons cm^{-2} with the ice as deposited; (*b*) 1.9×10^{18} with 6.5×10^{18} photons cm^{-2}.

4. Astrophysical implications

Solid-state abundances of NH_2CHO molecule can be predicted from gas-grain chemical models only when a complete picture of its formation and destruction under different conditions are taken into account. A knowledge of the corresponding rates related to the cross-sections is therefore necessary. Formamide ice could most likely be present in the dense interstellar cloud conditions not in a pure form but mixed with water or other interstellar ice components. However, formamide is more refractory than water or other volatiles, which means that small quantities of pure formamide ice could exist in elevated grain temperatures. In addition, to determine the extent of destruction under various energetic processing agents and to compare their effects, here we have considered a pure ice as done in previous studies. Dawley et al. (2014a) showed that H_2O plays a catalytic role by increasing the product formation when H_2O mixed NH_2CHO ice is exposed to Lyα photons. However, the impact of other volatiles is still unknown and would require dedicated experiments to gain further insight.

In fact, in an earlier study, we derived the effective destruction cross-section, $\sigma_{d,H} = 3.0 \pm 0.6 \times 10^{-17}$ cm^2 for pure NH_2CHO due to thermal H atom exposure. This was found to be an order of magnitude lower than that derived for the destruction of formamide by 200 keV H^+, simulating the effects of cosmic rays. Under the approximation of monoenergetic 1 MeV protons, a value of $\sigma_{d,1\,MeV} = 3.7 \pm 0.4 \times 10^{-16}$ cm^2, was derived (Baratta & Palumbo, priv. comm.). Furthermore, due to the lack of experimentally derived NH_2CHO destruction cross-section under Lyα (10.2 eV) photons, we made the decision to derive only an upper limit value of the destruction cross-section, $\sigma_{UV} = 7.5 \times 10^{-16}$ cm^2. We argued that high energy protons would induce multiple bond breaking in the molecules along the "hot track"[1] compared to a single photolysis step by Lyα photons and therefore the UV destruction cross-section should be lower than that for energetic protons. In agreement with the above argument, we found that the UV destruction cross-section of formamide, $\sigma_{d,UV} = 1.9 \pm 0.2 \times 10^{-18}$ cm^2, estimated in

[1] The path of the swift ions through the ice film which gets locally heated from the energy of the ions.

Table 2. Destruction cross-sections of NH_2CHO under different energetic processing and the corresponding rates in the dense interstellar clouds.

Processing	Destruction cross-section σ_d, (cm^2)	Flux Φ, ($cm^{-2}\,s^{-1}$)	Destruction rate R_d, (s^{-1})
UV photons	$1.9 \pm 0.2 \times 10^{-18}$	4.8×10^3 [c]	9.1×10^{-15}
H atoms	$3.0 \pm 0.6 \times 10^{-17}$ [a]	9.1×10^4 [b]	2.7×10^{-12}
Cosmic rays	$3.7 \pm 0.4 \times 10^{-16}$ [d]	1 [e]	3.7×10^{-16}

Notes. [a]Suhasaria & Mennella (2020). [b]Mennella (2006). [c]Corresponds to 10 eV photons (Mennella et al. 2003). [d]Corresponds to 1 MeV protons under monoenergetic approximation (Baratta & Palumbo, priv. comm.) [e]Mennella et al. (2003).

the present work, is two orders of magnitude lower than that obtained for energetic protons. Moreover, $\sigma_{d,UV}$ is about ten times lower than $\sigma_{d,H}$, the destruction cross-section by H atoms (see Table 2).

The derivation of the cross-section further allowed us to evaluate the NH_2CHO destruction rate under UV photons in dense clouds and to compare it with the destruction rates induced by H atoms and cosmic rays. In the dense cloud cores, formamide ice should be shielded from the external UV radiation but there are locally produced UV rays resulting from cosmic-ray induced ionisation of hydrogen. The energy of the UV photons that impinges on the interior of dense clouds resembles the Lyα. Taking into account the UV photons flux of 4.8×10^3 $cm^{-2}\,s^{-1}$ (Mennella et al. 2003) in those environments, the destruction rate of $R_d = 9.1 \times 10^{-15}\,s^{-1}$ was obtained. Although this rate was found to be an order of magnitude higher than the cosmic rays, the rate was still three orders of magnitude lower than that induced by H atoms. This means that H atoms induce the higher destruction efficiency in formamide compared to UV photons or cosmic rays in those environments. The destruction rates for formamide under different energetic processing are also given in Table 2.

5. Conclusions

This experimental study of Lyα irradiation of NH_2CHO ice at 12 K under high vacuum conditions is intended to improve our understanding of its photo stability under dense cloud conditions. The UV photolysis results in the formation of new products: CO, NH_4^+ OCN^-, HCN, HNCO, and CO_2, which were identified by FTIR spectroscopy. The formation mechanism of other photo products is also discussed in this work. The destruction of N–H, C–H, and C=O functional groups in NH_2CHO occurred in a single step, unlike the case of H atom bombardment, as examined in our previous study. For the first time, the Lyα destruction cross-section of NH_2CHO and the cumulative formation cross-section of different photo products have been estimated. The comparison of the destruction rate of NH_2CHO in dense clouds obtained in the present work with those induced by other processes indicates that interaction among H atoms remains the driving mechanism leading to the destruction of this molecule in those environments.

Acknowledgements. This work has been supported by the project PRIN-INAF 2016 "The Cradle of Life- GENESIS- SKA" (General Conditions in Early Planetary Systems for the rise of life with SKA). The authors wish to thank Angela Ciaravella and Antonio Jimenez Escobar for fruitful discussions.

References

Altwegg, K., Balsiger, H., Berthelier, J.-J., et al. 2017, MNRAS, 469, S130
Bisschop, S. E., Jørgensen, J., Van Dishoeck, E., & De Wachter, E. 2007, A&A, 465, 913
Biver, N., Bockelée-Morvan, D., Debout, V., et al. 2014, A&A, 566, L5
Blake, G. A., Sutton, E., Masson, C., & Phillips, T. 1986, ApJS, 60, 357
Bockelée-Morvan, D., Lis, D., Wink, J., et al. 2000, A&A, 353, 1101
Botta, L., Saladino, R., Bizzarri, B. M., et al. 2018, Adv. Space Res., 62, 2372
Brucato, J., Strazzulla, G., Baratta, G., Rotundi, A., & Colangeli, L. 2006a, J. Int. Astrobiol. Soc., 36, 451
Brucato, J. R., Baratta, G. A., & Strazzulla, G. 2006b, A&A, 455, 395
Chuang, K.-J., Fedoseev, G., Scirè, C., et al. 2021, A&A, 650, A85
Corazzi, M. A., Fedele, D., Poggiali, G., & Brucato, J. R. 2020, A&A, 636, A63
Couturier-Tamburelli, I., Piétri, N., Le Letty, V., Chiavassa, T., & Gudipati, M. 2018, ApJ, 852, 117
Dawley, M. M., Pirim, C., & Orlando, T. M. 2014a, J. Phys. Chem. A, 118, 1228
Dawley, M. M., Pirim, C., & Orlando, T. M. 2014b, J. Phys. Chem. A, 118, 1220
Duvernay, F., Trivella, A., Borget, F., et al. 2005, J. Phys. Chem. A, 109, 11155
Ferus, M., Kubelik, P., & Civis, S. 2011, J. Phys. Chem. A, 115, 12132
Ferus, M., Nesvorný, D., Šponer, J., et al. 2015, Proc. Natl. Acad. Sci., 112, 657
Gerakines, P., Moore, M., & Hudson, R. 2004, Icarus, 170, 202
Gerakines, P. A., Yarnall, Y. Y., & Hudson, R. L. 2022, MNRAS, 509, 3515
Gibb, E., Whittet, D., Boogert, A., & Tielens, A. 2004, ApJS, 151, 35
Gingell, J., Mason, N., Zhao, H., Walker, I., & Siggel, M. 1997, Chem. Phys., 220, 191
Goesmann, F., Rosenbauer, H., Bredehöft, J. H., et al. 2015, Science, 349, aab0689
Haupa, K. A., Tarczay, G., & Lee, Y.-P. 2019, J. Am. Chem. Soc., 141, 11614
Jiang, G. J., Person, W. B., & Brown, K. G. 1975, J. Chem. Phys., 62, 1201
López-Sepulcre, A., Jaber, A. A., Mendoza, E., et al. 2015, MNRAS, 449, 2438
López-Sepulcre, A., Balucani, N., Ceccarelli, C., et al. 2019, ACS Earth Space Chem., 3, 2122
Lundell, J., Krajewska, M., & Räsänen, M. 1998, J. Phys. Chem. A, 102, 6643
Maier, G., & Endres, J. 2000, Eur. J. Org. Chem., 2000, 1061
Mendoza, E., Lefloch, B., López-Sepulcre, A., et al. 2014, MNRAS, 445, 151
Mennella, V. 2006, ApJ, 647, L49
Mennella, V., Baratta, G., Esposito, A., Ferini, G., & Pendleton, Y. 2003, ApJ, 587, 727
Mennella, V., Baratta, G. A., Palumbo, M. E., & Bergin, E. A. 2006, ApJ, 643, 923
Modica, P., & Palumbo, M. E. 2010, A&A, 519, A22
Nguyen, V. S., Abbott, H. L., Dawley, M. M., et al. 2011, J. Phys. Chem. A, 115, 841
Raunier, S., Chiavassa, T., Duvernay, F., et al. 2004a, A&A, 416, 165
Raunier, S., Chiavassa, T., Marinelli, F., & Aycard, J.-P. 2004b, Chem. Phys., 302, 259
Saladino, R., Crestini, C., Pino, S., Costanzo, G., & Mauro, E. D. 2012, Phys. Life Rev., 9, 84
Suhasaria, T., & Mennella, V. 2020, A&A, 641, A88
Turner, B. 1991, ApJS, 76, 617
Van Broekhuizen, F. A., Keane, J. V., & Schutte, W. A. 2004, A&A, 415, 425
Watanabe, N., & Kouchi, A. 2002, ApJ, 571, L173
Yamada, H., & Person, W. B. 1964, J. Chem. Phys., 41, 2478